ADVANCED FUNCTIONAL MATERIALS
www.afm-journal.de

Thermal Conductivity and Phonon Scattering Processes of ALD Grown PbTe–PbSe Thermoelectric Thin Films

*Mallory E. DeCoster, Xin Chen, Kai Zhang, Christina M. Rost, Eric R. Hoglund, James M. Howe, Thomas E. Beechem, Helmut Baumgart, and Patrick E. Hopkins**

This work studies the thermal conductivity and phonon scattering processes in a series of n-type lead telluride-lead selenide (PbTe–PbSe) nanostructured thin films grown by atomic layer deposition (ALD). The ALD growth of the PbTe–PbSe samples in this work results in nonepitaxial films grown directly on native oxide/Si substrates, where the Volmer–Weber mode of growth promotes grains with a preferred columnar orientation. The ALD growth of these lead-rich PbTe, PbSe, and PbTe–PbSe thin films results in secondary oxide phases, along with an increase microstructural quality with increased film thickness. The compositional variation and resulting point and planar defects in the PbTe–PbSe nanostructures give rise to additional phonon scattering events that reduce the thermal conductivity below that of the corresponding ALD-grown control PbTe and PbSe films. Temperature-dependent thermal conductivity measurements show that the phonon scattering in these ALD-grown PbTe–PbSe nanostructured materials, along with ALD-grown PbTe and PbSe thin films, are driven by extrinsic defect scattering processes as opposed to phonon–phonon scattering processes intrinsic to the PbTe or PbSe phonon spectra. The implication of this work is that polycrystalline, nanostructured ALD composites of thermoelectric PbTe–PbSe films are effective in reducing the phonon thermal conductivity, and represent a pathway for further improvement of the figure of merit (*ZT*), enhancing their thermoelectric application potential.

1. Introduction

Nanostructured semiconductors continue to be pursued for thermoelectric applications owing to their potential for increased thermoelectric figure of merit, ZT, through enhancements to the power factor ($S^2\sigma$) with simultaneous reductions to the contribution of the lattice thermal conductivity.[1,2] Lead selenide (PbSe) and lead telluride (PbTe) are promising semiconducting materials for this application[3] due to their intrinsically high figure of merit (ZT), low vapor pressure, and high melting point. Therefore, significant efforts have focused on improving the thermoelectric properties of bulk and nanostructured PbTe- and PbSe-based materials.[4–8] An improved Seebeck effect has been measured in atomic layer deposition (ALD) grown lead-rich n-type PbTe–PbSe nanolaminates in both the cross and in-plane directions, which was attributed to changes in the electronic density of states from the nanostructuring and off-stoichiometry.[4] Additionally, first-principles calculations have shown that nanostructures separated by less than ≈20 nm could favorably scatter phonons within pure PbSe and PbTe.[9] Taken together, nanostructuring and chemical modification to PbSe- and PbTe-based films with defect and interface length scales less than, or on the order, of a few tens of nanometers may therefore present an opportunity for enhanced thermoelectric performance. Here, we assess this hypothesis through a detailed experimental study of the phonon scattering mechanisms and thermal transport properties of a series of ALD grown PbTe–PbSe nanostructured thin films.

Here, we examine the impact of limiting length scales on phonon heat transport mechanisms within thermoelectric

M. E. DeCoster, Prof. C. M. Rost,[+] Prof. P. E. Hopkins
Department of Mechanical and Aerospace Engineering
University of Virginia
Charlottesville, VA 22904-4746, USA
E-mail: phopkins@virginia.edu
Dr. X. Chen, Dr. K. Zhang, Prof. H. Baumgart
Department of Electrical Computer Engineering
Old Dominion University
Norfolk, VA 23529, USA
The ORCID identification number(s) for the author(s) of this article can be found under https://doi.org/10.1002/adfm.201904073.
[+]Present address: Department of Physics & Astronomy, James Madison University, Harrisonburg, VA 22807, USA
E. R. Hoglund, Prof. J. M. Howe, Prof. P. E. Hopkins
Department of Materials Science and Engineering
University of Virginia
Charlottesville, VA 22904-4746, USA
Dr. T. E. Beechem
Applied Optical Plasma Sciences
Sandia National Laboratories
Albuquerque, NM 87123, USA
Prof. P. E. Hopkins
Department of Physics
University of Virginia
Charlottesville, VA 22904-4746, USA

DOI: 10.1002/adfm.201904073

PbTe–PbSe nanosystems. We study the thermal transport processes in a series of ALD deposited, Pb-rich, PbTe–PbSe nanostructured thin films. Our ALD method of growth allows for layering during deposition that results in polycrystalline thin films with laminate and alloy features throughout the film thickness. The various nanostructures (grain boundaries, PbTe–PbSe layering, and compositional defects) result in polycrystalline films that follow disorder-like trends in their thermal conductivities, which are preferential for thermoelectric applications. We attribute these low phonon thermal conductivities to the various point and planar defects that are inherent to the growth of these ALD-grown films.

It is well known that nanostructuring in thin films and superlattices (SLs) at a few to tens of nanometer length scales can significantly reduce thermal conductivity relative to their bulk counterparts.[2,6,10–17] This is consistent with other phonon dominated systems where size effects emerge at the microscale.[18–24] Electron dominated systems, in contrast, are more often unaffected by size until limited at the nanometer scale.[22,25,26] Generally, in systems where the average mean free path of phonons is longer than the limiting dimension of the sample, the heat transport fails to follow Fourier's law and can instead be described by semiballistic phonon transport; in this regime, the wave nature of phonons can appear, possibly preserving coherence.[13,24–27]

The interplay of quantum size effects from coherent transport (where a reduced Brillouin zone introduces phonon band gaps that reduce the phonon group velocity and the phonon scattering phase space) and incoherent size effects (where phonons scatter diffusively at internal interfaces) has been extensively studied in many material systems including: Si/Ge, GaAs/AlAs, BiTe/SbTe, and $SrTiO_3/CaTiO_3$ superlattices.[10,13,26–29] In these systems, the periodicity of the superlattice is thought to affect the thermal conductivity in two ways: i) it creates well-defined internal boundaries that increase phonon boundary scattering (i.e., incoherent) or ii) the phonons see the periodicity of the SL as a new material, resulting in a modified phonon dispersion (i.e., coherent).[25] The thermal conductivity trends in periodicity and film thickness can be indicators of coherent-phonon transport impacting thermal transport. In the case of our current study, we find that while the thickness dependent trends in the PbTe–PbSe samples' thermal conductivities are similar to those found in alloys and SLs dominated by long wavelength, possible coherent phonon transport,[13,14,30–33] our samples' thermal conductivity thickness trends are dictated by spatially varying defect densities, where thicker films result in higher quality samples.

In this work, we report on the cross plane thermal conductivity of PbTe–PbSe nanostructured, polycrystalline thin films. We measure the thermal conductivity over a range of temperatures using time domain thermoreflectance (TDTR); with a combination of atomic force microscopy (AFM), scanning electron microscopy (SEM), transmission electron microscopy (TEM), X-ray diffraction (XRD), energy dispersive X-ray (EDS) spectroscopy, and Raman spectroscopy. We find that the phonon thermal transport processes in these ALD-grown films are determined by: i) thickness varying crystalline quality, where structural defect densities increase in thinner films due to the ALD growth mode of these materials; ii) point defects inherent in the ALD growth process (e.g., oxygen defects); and iii) compositional-driven defects, such as point defects and phase boundaries between the PbTe and PbSe.

2. Results and Discussion

The nanostructured PbTe–PbSe thin films were grown via ALD as discussed previously.[4] During the ALD growth, we varied the pulse time of the PbTe and PbSe precursors, as described elsewhere,[4] to promote nanolaminate PbTe–PbSe texturing and spatial variation of the chemical composition. The ALD deposition of PbTe, PbSe, and PbTe–PbSe nanocomposite films does not follow a classical growth mode of monolayer upon monolayer, but grows in the initial incubation phase by heterogeneous nucleation as an expanding conglomerate of island clusters (Volmer–Weber growth), leading to polycrystalline PbTe and PbSe rather than amorphous films. This Volmer–Weber island growth mode is a result of the fact that the optimized ALD deposition temperature of 150 °C is above the crystallization temperature, and first and foremost, the lead selenide and telluride ALD precursor atoms bond more strongly with one another than to the surface and exhibit weaker substrate chemisorption. Deposition at 150 °C leads to immediate crystallization into nanoscale cubic nuclei, which rules out amorphous films.

The structural and chemical length scales and heterogeneity of these films are characterized via XRD, TEM, and EDS, shown in **Figure 1**. XRD data shown in Figure 1a indicates the presence of polycrystalline PbTe and PbSe in all samples (compositionally homogeneous "control" films and compositionally heterogeneous "nanostructured" films) where the growth direction is predominantly along the <200> crystallographic direction. Corresponding Williamson–Hall analysis (Supporting Information) shows that the crystalline coherent length and domain sizes in these samples increase with film thickness, indicating an increase in film quality as the sample thickness increases, which is an expected outcome from the Volmer–Weber growth. Additional crystallinity and film quality characterization is discussed in the Supporting Information with respect to SEM, AFM, and TEM (Figures S5, S6, and S9, Supporting Information).

Figure 1b shows representative TEM of PbTe controls and nanostructured samples, further confirming the polycrystallinity. We observe grain sizes in the TEM of the PbTe control films on the order of 143–193 nm and in nanocomposites on the order of 48–96 nm, which is further supported by the SEM in Figure S5 (Supporting Information). Further, we do not observe any evidence of consistent layering of PbTe and PbSe throughout the film thickness, which we confirm with fast Fourier transform (FFT) image analysis of the TEM micrographs (Figure 1c). Corresponding EDS analysis (Figure 1d and Figures S7 and S8 in the Supporting Information) shows that the composition and stoichiometry of both the control and nanostructured films are lead rich, consistent with previous work,[4] and also indicative of n-type semiconductors necessary for improved thermoelectric response in these systems; thus, our samples are nonstoichiometric with elemental compositions of selected samples

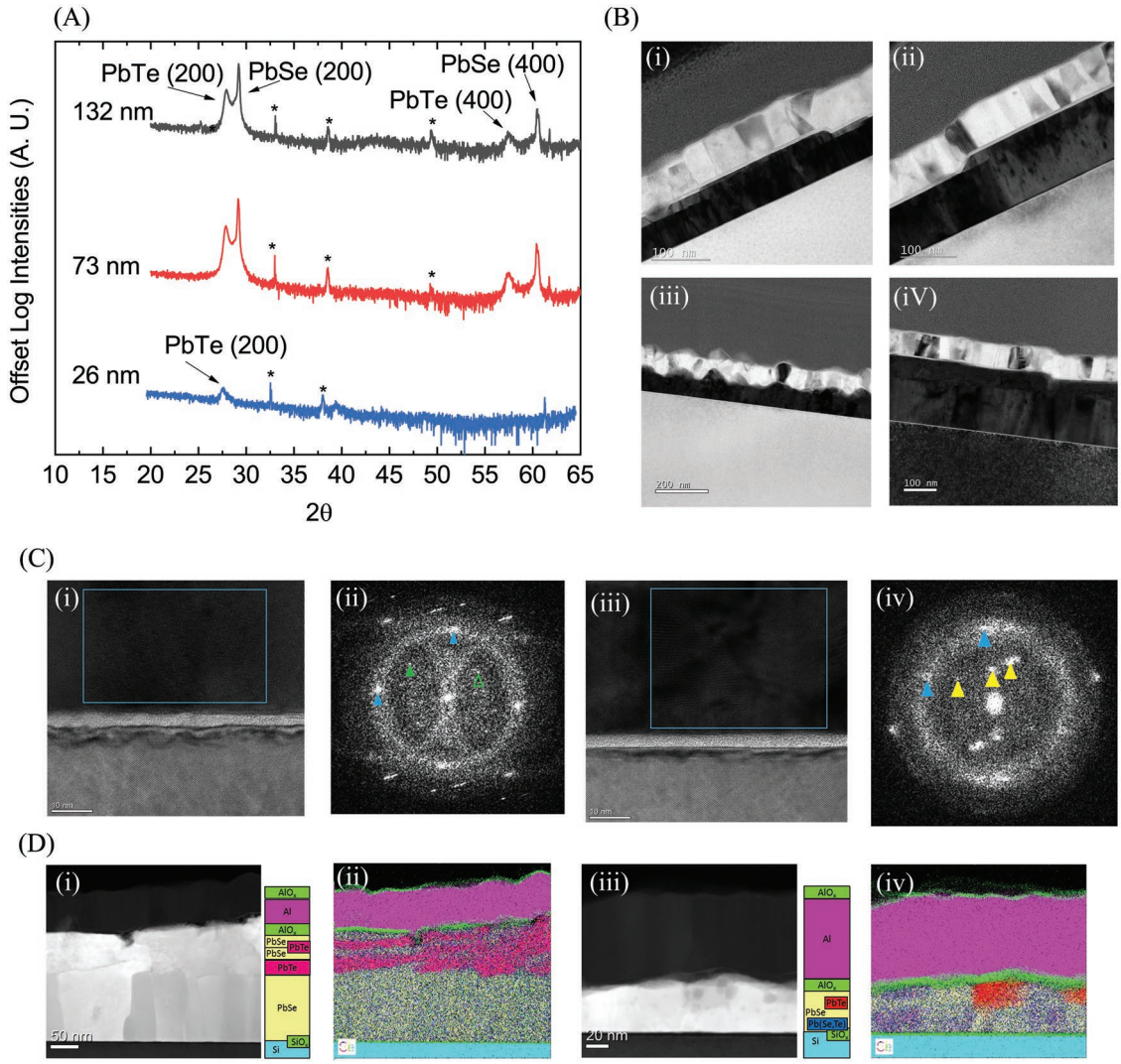

Figure 1. A) X-ray Diffraction (XRD) of the PbTe–PbSe nanocomposite samples for different total thicknesses. The additional peaks in the spectra labeled by stars are indicative of secondary lead oxide phases. Note the 26 nm sample only has a clear peak for the PbTe phase and not the PbSe. PbSe peaks are nonexistent due to the reduction in the measurement volume. B) HR-TEM data for i) 77 nm PbTe with an average grain size of 143 ± 31 nm; ii) 105 nm PbTe with an average grain size of 193 ± 64 nm; iii) 73 nm PbTe–PbSe nanocomposite with an average grain size ≤100 nm; and iv) 196 nm PbTe–PbSe with and average grain size ≥150 nm. C) i) HR-TEM and ii) FFT from the 188 nm PbTe–PbSe film section of the HR-TEM that shows inter planar spacings of 0.309 (blue arrows), 0.432 (solid green arrow), and 0.552 (hollow green arrow) nm. The 0.309 and 0.432 nm spacing relate to the 002 and 011 planes of PbSe. iii) HR-TEM and iv) FFT from the 55 nm PbTe–PbSe film that shows inter planar spacings of 0.312 nm (blue arrows), which is in between the 002 spacing of PbSe and PbTe. Reciprocal space peaks indicated by yellow arrows result from Moiré fringes. No superlattice periodicities were observed in either FFT. The blue squares show the area in which the FFT was taken. D) EDS data for i,ii) 188 nm thick and iii,iv) 60 nm thick PbTe–PbSe films, where (i,iii) shows the EDS HAADF cross sectional image, (ii,iv) shows the distribution of Al (pink), O (green), Te (red), Se (yellow), Pb (blue), and Si (aqua). We include a schematic to the left of each EDS image to further exemplify the morphology of the samples, where we see two wavelengths of layering at the top of the 188 nm sample, while the 60 nm sample exhibits a granular structure.

indicated in Figure 1d. Further, our XRD and EDS confirm the presence of lead oxide, not only at the film surfaces but also internal to the films.

Thus, our characterization presented in Figure 1 and Figures S5–S18 in the Supporting Information confirms the presence of a multitude of different types of defects common in all the control and nanostructured films, including: Pb-oxide defects from the growth conditions, grain boundaries from the Volmer–Weber island growth mode, compositional boundaries from chemical segregation of the PbTe and PbSe phases, and additional planar defects that we characterize under a crystalline coherence length change from XRD and Raman analysis (most likely, these additional defects are in the form of dislocation or additional domain boundaries from any localized PbTe–PbSe layering effects, discussed in the Supporting Information). Taken together, the ALD grown thermoelectric PbTe–PbSe films studied in this work all have common point defects among the various samples, but the crystalline quality of all films increase with increasing film thickness, indicative of larger spacing between structural

planar defects, which is expected from the Volmer–Weber growth mode.

Figure 1 shows the XRD, TEM (and corresponding FFT image analysis), and EDS data for a thin and thick PbTe–PbSe nanocomposite. The XRD data are plotted as a function of thickness and show evidence of peak broadening as the total thickness is reduced, corresponding to a reduction in film quality. This analysis is provided in more detail in the Supporting Information. Additionally, it is important to elaborate on the role of the lead oxide that is present in the XRD data in Figure 1a. Additional characterization by EDS (Figure 1d and Figures S7 and S8, Supporting Information) show the presence of PbO occurs both at the front and backside surfaces and within the films (however we cannot confirm that the PbO layer is confined to the sample surface since TEM is a projection). The PbO that is internal to the material will play a large role, acting as point defects to scatter phonons and reduce the thermal conductivity of the films. Figure 1b shows high resolution TEM of a thick and thin PbTe control film and nanocomposite, where the oriented grains are clearly visible. Indexing of the inter planar spacings of the FFT of the high-resolution transmission electron microscopy (HR-TEM) in Figure 1c does not indicate evidence of superlattice periodicities in either sample. Figure 1d shows the EDS data which illuminates the morphology of the Pb, Te, Se, and O within the films. We see evidence of nanocomposite grains of PbTe and PbSe within both films, with some rough periodic layering occurring in the thicker sample.

We measured the thermal conductivities of the PbTe–PbSe nanostructured thin films, as well as the control ALD-grown thin films of PbTe and PbSe with TDTR. The samples and thicknesses are listed in Table S1 in the Supporting Information, along with the measured thermal conductivities. **Figure 2** plots the thermal conductivity as a function of total film thickness for the various PbTe–PbSe thin films. For comparison, we also plot the thermal conductivity as a function of target PbTe/PbSe layer thickness during growth in Figure S1b (Supporting Information). As previously mentioned, we see no evidence of consistent SL-like layering in our ALD-grown samples, however, we do observe compositional segregation and heterogeneity on the order of tens of nanometers, along with grain boundaries on this length scale. The thermal conductivities of these PbTe–PbSe films increase with total film thickness, which is discussed in more detail below. Additionally, we observe no apparent trend in target PbTe/PbSe layer thicknesses (cf., Table S1 and Figure S1, Supporting Information), which is most likely due to the diffusive spatial gradation of the chemical composition between the two nanolaminate compounds. Note, period independence in the thermal conductivity of PbTe/PbSe SLs has been observed previously in molecular beam epitaxy (MBE) grown $(PbTe)_{1-x}/(PbSe)_x$ nanodot superlattices (NDSLs) from periods from 5 to 50 nm.[7] This periodic independence was partially ascribed to the fact that the nanodot layers in these aforementioned NDSLs did not form well-defined layers. This is consistent with our current ALD-grown samples, and the lack of observable superlattice-like layering in our films.

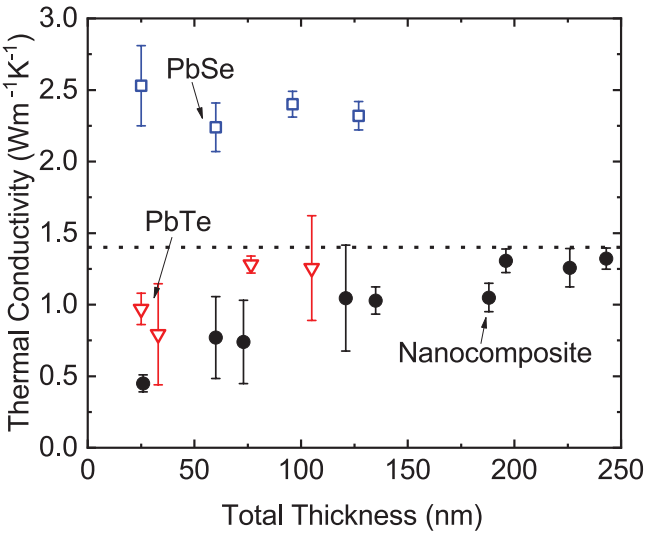

Figure 2. Thermal conductivity results for the PbTe and PbSe control and PbTe–PbSe nanocomposite materials versus total sample thickness. The dotted line represents calculations using Equation (1) (a series resistor model).

In general, the thermal conductivities of the nanostructured films are lower than those of the control thin films. The control PbSe films do not exhibit size effects, while the PbTe controls seem to experiences size effects over the thickness range studied (a 40% increase in thermal conductivity when the film increases from 25 to 120 nm). This reduction is not a traditional size effect (increased boundary scattering), but due to the thickness-varying structural defects that occur during ALD growth of the PbTe layer. Our thermal conductivity results suggest that this same thickness-varying film quality is not occurring in the PbSe layers. Additionally, the thermal conductivity of the thick PbTe–PbSe nanostructured films (≥121 nm) are relatively constant with total thickness, but still show a reduction in thermal conductivity compared to the control films. Increased phonon scattering due to varying compositional point defects (i.e., Te and Se) and compositional phase boundaries between the PbTe and PbSe (or other planar defects originating from the compositional variation, like dislocations) is likely contributing to the relatively reduced thermal conductivity of the nanostructured films in this thickness regime (cf., TEM and EDS analysis in Figure 1), where film quality has been maximized. However, in the thin film regime, the Volmer–Weber growth plays a major role in further reducing the thermal conductivity of the nanostructured films as the sample thickness is reduced and concomitantly the sample quality is degraded. Thus, we ascribe the reduction in thermal conductivity of the nanostructured thin films compared to the parent materials due to compositional effects (point and planar defects driven by the spatially varying chemical composition). The film thickness dependent thermal conductivity of the nanostructured film and PbTe control film is driven by an increased microstructural quality with increased film thickness.

While the film qualities, microstructures and chemical composition of the various samples were studied with a range of techniques discussed in Figure 1 and in the Supporting Information to semiquantitatively assess the varying film quality with sample thickness in the control films, we turn to Raman Spectroscopy to further highlight the reduction in film order with thickness.

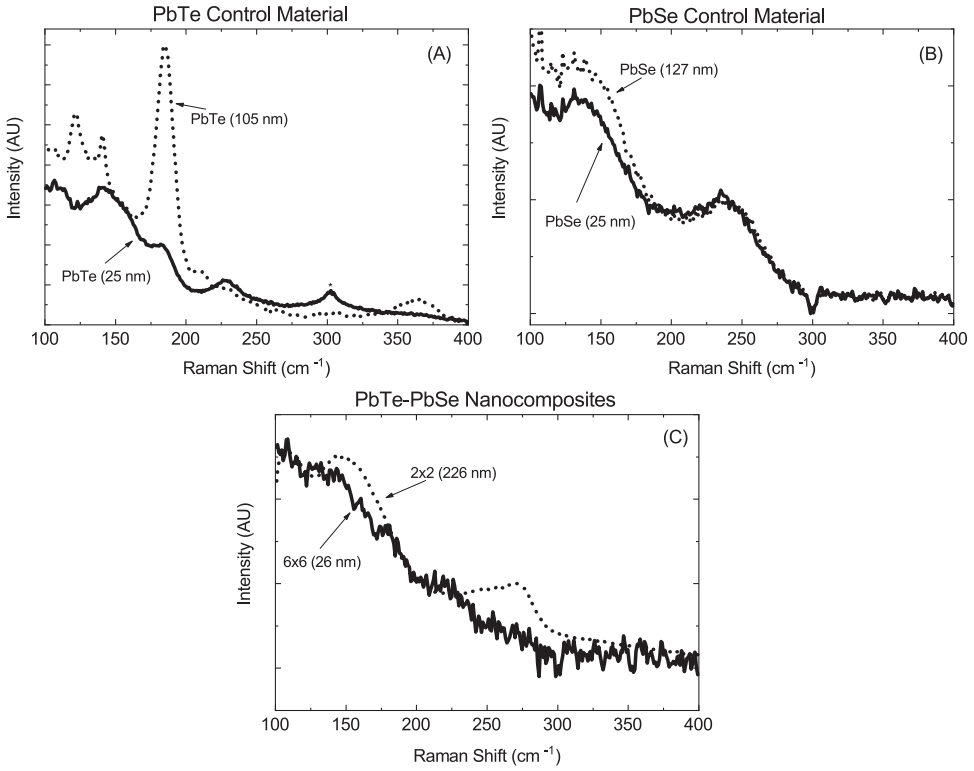

Figure 3. Raman spectra of a thin and thick film for: A) PbTe, B) PbSe, and C) nanocomposites. Linewidth increases in the thinner PbTe and nanocomposite films owing to increased disorder.

Raman spectra for thick and thin parent materials and accompanying nanocomposites of varying thicknesses are displayed in **Figure 3**. Spectra are scaled to allow for comparison. In some cases, the background signal originating from the second order acoustic overtones of Si has been removed via subtraction.[34] Mode positions are consistent with expectation for the films.[35] The linewidth of the peaks varies significantly depending on total film thickness for both the PbTe control films and the nanocomposites, whereas no substantial change occurs to the PbSe controls. All told, these variations in linewidth with thickness further corroborate the reduction in film quality with reduced thickness that occurs as a consequence of the Vollmer–Weber growth.[9,44]

First-principles calculations have shown that a large portion of heat conducted in PbTe and PbSe is carried by phonons with a distribution of mean free paths that are ≤10 nm.[9,36,44] If these phonons scatter diffusively at the compositional phase boundaries in the nanostructured films (as suggested by the lack of trend in thermal conductivity vs target layer thickness during growth, shown in Table S1 and Figure S1, Supporting Information), then the dominant heat transport picture can be described by a coherence length and mean free path that are smaller than the period thickness, so that the wave packet is only located in one material and experiences many phonon–phonon collisions before scattering at the internal interfaces.[37] Assuming relatively negligible thermal boundary resistances at the compositional interfaces, the thermal conductivity of the nanostructured films would be a weighted average of the thermal resistivities of the two parent materials represented as a series resistor according to[31]

$$\frac{1}{\kappa_{\text{nanostructure}}} = \frac{1}{d_1 + d_2}\left(\frac{d_1}{\kappa_1} + \frac{d_2}{\kappa_2}\right) \quad (1)$$

where, d_1 and d_2 are the thicknesses of the parent materials and κ_1 and κ_2 are the thermal conductivities of the respective parent materials. We take the intrinsic thermal conductivities of the parent material to be the values measured for the thinnest samples (25 nm), and plot the result of Equation (1) in Figure 2 as a dotted line. This model sets the upper bound on the thermal conductivity of a superlattices when boundary and defect scattering are not playing a role. The reduction of thermal conductivity below this threshold suggests that additional scattering mechanisms are playing a role in reducing the thermal transport below that of the control materials, which we ascribe to the spatially varying compositional variations of PbTe and PbSe leading to both chemical heterogeneity of Se and Te and PbTe/PbSe phase boundaries, as discussed with respect to Figure 1.

To gain further insight into the phonon scattering mechanisms driving the thermal conductivity in these ALD-grown PbTe–PbSe thermoelectric films, we measure the thermal conductivity of the highest and lowest thermal conductivity control films (127 nm thick PbSe film and 33 nm thick PbTe film—cf., Figure 2 and Table S1, Supporting Information), and the thermal conductivity of a 121 nm thick PbTe–PbSe nanostructure film as a function of temperature from 77 to 298 K. **Figure 4** shows the temperature-dependent trends of these three ALD grown samples, compared to experimental data for bulk samples of PbSe[38] and PbTe[39] from literature. The thin film control and nanostructure films show an increase in thermal conductivity with an increase in temperature. This is in contrast

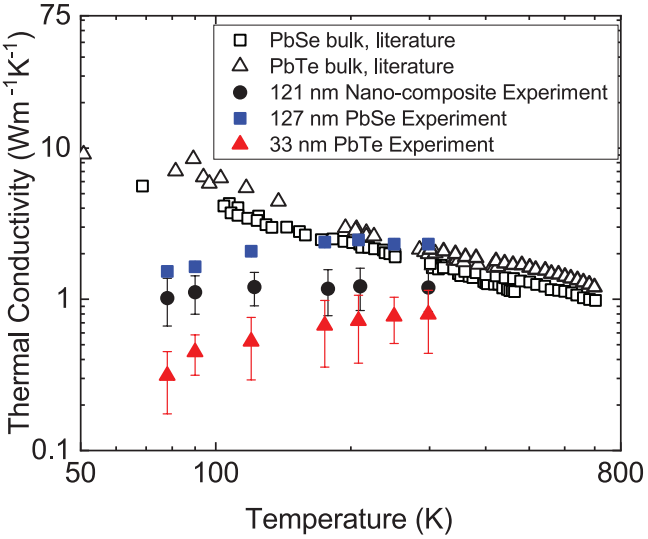

Figure 4. Thermal conductivity versus temperature for PbSe (127 nm sample thickness), PbTe (33 nm sample thickness), and a PbTe–PbSe nanocomposite (121 nm sample thickness) with a 20 nm compositional period thickness. Data collected on bulk samples are taken from the literature for PbSe[38] and PbTe.[39] The temperature-dependent thermal conductivity trends in our ALD-grown samples indicate that the phonon scattering processes are driven by extrinsic defect scattering processes as opposed to phonon–phonon scattering processes intrinsic to the PbTe or PbSe phonon spectra.

to the temperature-dependent thermal conductivity of the bulk counterparts, which show a $1/T$ trend that is typical of increased Umklapp scattering in crystalline solids. From our TEM and EDS data previously discussed (Figure 1d and Figures S7 and S10, Supporting Information), these thermal conductivity trends are reasonable given the high levels of chemical point defects in the samples (e.g., Pb–O defects in the control and nanostructured samples) and structural defects from the Volmer–Weber growth process. Thus, the phonon scattering and resulting thermal conductivities in these ALD-grown PbTe–PbSe thermoelectric materials are driven by extrinsic defect scattering processes as opposed to phonon–phonon scattering processes intrinsic to the PbTe or PbSe phonon spectra.

The thin films follow the temperature-dependent heat capacity trend of classic kinetic theory, given by,

$$\kappa = \frac{1}{3}\sum_i C_i \upsilon_i l_i \tag{2}$$

The summation in Equation (2) is performed over all the available vibrational modes (i), C_i is the heat capacity, υ_i is the group velocity, and l_i is the phonon mean free path. This trend implies that three phonon scattering plays a minor role in the thermal conductivity of these films, even in the control materials, since there is no evidence of the temperature-dependent thermal conductivity trends expected from phonon–phonon scattering, as previously mentioned. Further, the temperature-dependent thermal conductivity trend of the nanostructure film is reduced compared to the PbSe control film with a similar thickness, consistent with a reduction in l_i from the various additional phonon scattering mechanisms in these nanostructures, as previously discussed.

3. Conclusion

In conclusion, the ALD growth of the PbTe–PbSe thermoelectric samples in this work resulted in nonepitaxial films grown directly on native oxide/Si substrates, where the Volmer–Weber mode growth promoted the growth of grains with a preferred columnar orientation, secondary oxide phases that acted as point defects within the films, and increased microstructural quality with increased film thickness. We find that the phonon thermal transport processes in these ALD-grown films are determined by: i) thickness varying crystalline quality, where structural defect densities increase in thinner films due to the ALD growth mode of these materials; ii) point defects inherent in the ALD growth process (e.g., oxygen defects); and iii) compositional-driven defects, such as point defects and phase boundaries between the PbTe and PbSe. While nanoscale superlattice structures are not observed in our PbTe–PbSe systems, the compositional variation and resulting point and planar defects give rise to additional phonon scattering events that reduce the thermal conductivity below that of the corresponding ALD-grown control PbTe and PbSe films. Temperature-dependent thermal conductivity measurements further support our findings that the phonon scattering and resulting thermal conductivities in these ALD-grown PbTe–PbSe thermoelectric materials are driven by extrinsic defect scattering processes as opposed to phonon–phonon scattering processes intrinsic to the PbTe or PbSe phonon spectra. The implication of this work is that polycrystalline, nanostructured ALD composites of thermoelectric PbTe–PbSe films are effective in reducing the phonon thermal conductivity, and hereby represent a pathway for further improvement of the figure of merit (ZT), enhancing their thermoelectric application potential.

4. Experimental Section

Atomic Layer Deposition Sample Fabrication: The PbTe–PbSe polycrystalline, nonepitaxial films were fabricated by ALD using a Veeco Cambridge Nanotech Thermal ALD reactor. ALD is a robust method to synthesize PbTe–PbSe nanocomposite structures because it can precisely control the film layer thickness, composition, and uniformity.[40] The specifics of this technique have been published elsewhere.[4] Briefly, multiple layers of PbTe/PbSe were fabricated using $Pb(C_{11}H_{19}O_2)_2$ [lead(II)bis(2,2,6,6-tetramethyl3,5-heptanedionato)] as the lead precursor, $(Me_3Si)_2Te$, bis-(trimethylsilyl telluride) as the tellurium precursor, and $(Me_3Si)_2Se$ bis(trimethylsilyl selenide) as the selenium precursor. Inert N_2 (20 sccm) was used as the carrier gas to transport the chemical precursors into the ALD reaction chamber. The layering was targeted during growth of 2 nm/2 nm, 6 nm/6 nm, and 10 nm/10 nm PbTe/PbSe repeat units for the nanostructured films with total sample thicknesses ranging from 25 to 243 nm, deposited on native oxide covered planar (100)-oriented silicon substrates at a deposition temperature of 150 °C. Note, as described above, the evidence of PbTe/PbSe superlattice structures on these targeted layering length scales was not observed, but this approach led to spatial chemical heterogeneity and phase segregation/phase boundaries with length scales on the order of tens of nanometers. More detail is provided in the Supporting Information.

Thermal Measurements with TDTR: The thermal properties of these samples were measured by TDTR, which is described in detail elsewhere.[41,42] For the TDTR measurements, 80 ± 3 nm of aluminum was deposited on top of the superlattice samples by electron beam evaporation at a pressure of 1×10^{-6} Torr and a deposition rate of 1.0 Å s^{-1}. The 80 nm of Al served to transduce the optical energy from the TDTR laser pulses into thermal energy. TDTR is a time transient, noncontact,

optical thermometry technique that utilizes a pump–probe experimental configuration centered around the output of a sub-picosecond (ps) laser system. A Ti:Sapphire femtosecond Spectra Physics Tsunami oscillator was used that emitted 90 fs pulses at a repetition rate of 80 MHz with a wavelength centered at ≈800 nm (FWHM of 10.5 nm). Further, the pump path was electo-optically modulated with a square wave at a frequency of 10 or 3 MHz creating a modulated heating event at the sample surface. The reflectivity of the aluminum changed linearly with the surface temperature and this change in reflection was monitored temporally by the time delayed probe beam. The probe beam was mechanically delayed in time by a translational mechanical delay stage up to 5.5 ns. The reflected intensity from the probe was measured by a photodetector. A lock-in amplifier demodulated the signal and provided amplitude and phase data as a function of pump–probe delay time in the form of a thermal decay curve. These decay curves were fit with a heat conduction model to obtain the thermal properties of the sample.[42–44] The pump and probe $1/e^2$ diameters used in the measurements were 22 and 9.5 µm, respectively. See the Supporting Information for more details about the TDTR experiment.

Supporting Information

Supporting Information is available from the Wiley Online Library or from the author.

Acknowledgements

The authors appreciate funding from the Army Research Office, Grant No. W911NF-16-1-0406. This work was supported in part by the NSF I/UCRC on Multi-functional Integrated System Technology (MIST) Center IIP-1439644, IIP-1439680, and IIP-1738752.

Sandia National Laboratories is a multimission laboratory managed and operated by National Technology and Engineering Solutions of Sandia, LLC, a wholly owned subsidiary of Honeywell International Inc., for the U.S. Department of Energy's National Nuclear Security Administration under contract DE-NA0003525.

Conflict of Interest

The authors declare no conflict of interest.

Keywords

atomic layer deposition, chalcoginides, nanostructures, phonon scattering, thermal conductivity, Volmer–Weber growth

Received: May 21, 2019
Revised: July 29, 2019
Published online:

[1] A. J. Minnich, M. S. Dresselhaus, Z. F. Ren, G. Chen, *Energy Environ. Sci.* **2009**, *2*, 466.
[2] M. Zebarjadi, K. Esfarjani, M. S. Dresselhaus, Z. F. Ren, G. Chen, *Energy Environ. Sci.* **2012**, *5*, 5147.
[3] G. J. Snyder, E. S. Toberer, *Nat. Mater.* **2008**, *7*, 105.
[4] X. Chen, P. Lin, K. Zhang, H. Baumgart, B. Geist, V. Kochergin, *ECS J. Solid State Sci. Technol.* **2016**, *5*, 503.
[5] A. A. El-Sharkawy, A. M. Abou El-Azm, M. I. Kenawy, *Int. J. Thermophys.* **1983**, *4*, 261.
[6] T. C. Harman, P. J. Taylor, D. L. Spears, M. P. Walsh, *J. Electron. Mater.* **2000**, *29*, L1.
[7] Y. K. Koh, C. J. Vineis, S. D. Calawa, M. P. Walsh, D. G. Cahill, *Appl. Phys. Lett.* **2009**, *94*, 153101.
[8] J. M. Skelton, S. C. Parker, A. Togo, I. Tanaka, A. Walsh, *Phys. Rev. B* **2014**, *89*, 205203.
[9] Z. Tian, J. Garg, K. Esfarjani, T. Shiga, J. Shiomi, G. Chen, *Phys. Rev. B* **2012**, *85*, 184303.
[10] R. Venkatasubramanian, *Phys. Rev. B* **2000**, *61*, 3091.
[11] W. E. Bies, R. J. Radtke, H. Ehrenreich, *J. Appl. Phys.* **2000**, *88*, 1498.
[12] T. Borca-Tasciuc, W. Liu, J. Liu, T. Zeng, D. W. Song, C. D. Moore, G. Chen, K. L. Wang, M. S. Goorsky, *Superlattices Microstruct.* **2000**, *28*, 199.
[13] R. Cheaito, C. A. Polanco, S. Addamane, J. Zhang, A. W. Ghosh, G. Balakrishnan, P. E. Hopkins, *Phys. Rev. B* **2018**, *97*, 085306.
[14] R. Cheaito, J. C. Duda, T. E. Beechem, K. Hattar, J. F. Ihlefeld, D. L. Medlin, M. A. Rodriguez, M. J. Campion, E. S. Piekos, P. E. Hopkins, *Phys. Rev. Lett.* **2012**, *109*, 195901.
[15] B. Poudel, Q. Hao, Y. Ma, Y. Lan, A. Minnich, B. Yu, X. Yan, D. Wang, A. Muto, D. Vashaee, X. Chen, J. Liu, M. S. Dresselhaus, G. Chen, Z. Ren, *Science* **2008**, *320*, 634.
[16] B. F. Donovan, W. A. Jensen, L. Chen, A. Giri, S. J. Poon, J. A. Floro, P. E. Hopkins, *Appl. Phys. Lett.* **2018**, *112*, 213103.
[17] L. Chen, J. L. Braun, B. F. Donovan, P. E. Hopkins, S. J. Poon, *Appl. Phys. Lett.* **2017**, *111*, 131902.
[18] D. Song, G. Chen, *Appl. Phys. Lett.* **2004**, *84*, 687.
[19] K. Esfarjani, G. Chen, H. T. Stokes, *Phys. Rev. B* **2011**, *84*, 085204.
[20] A. J. Minnich, J. A. Johnson, A. J. Schmidt, K. Esfarjani, M. S. Dresselhaus, K. A. Nelson, G. Chen, *Phys. Rev. Lett.* **2011**, *107*, 095901.
[21] J. A. Johnson, A. A. Maznev, J. Cuffe, J. K. Eliason, A. J. Minnich, T. Kehoe, C. M. S. Torres, G. Chen, K. A. Nelson, *Phys. Rev. Lett.* **2013**, *110*, 025901.
[22] G. Chen, *Nanoscale Energy Transport and Conversion: A Parallel Treatment of Electrons, Molecules, Phonons, and Photons*, Oxford University Press, Inc., New York **2005**.
[23] A. M. Marconet, M. Asheghi, K. E. Goodson, *J. Heat Transfer* **2013**, *135*, 061601.
[24] T. E. Beechem, A. E. McDonald, E. J. Fuller, A. A. Talin, C. M. Rost, J.-P. Maria, J. T. Gaskins, P. E. Hopkins, A. A. Allerman, *J. Appl. Phys.* **2016**, *120*, 095104.
[25] P. E. Hopkins, J. R. Serrano, L. M. Phinney, H. Li, A. Misra, *J. Appl. Phys.* **2011**, *109*, 013524.
[26] P. E. Hopkins, P. M. Norris, L. M. Phinney, S. A. Policastro, R. G. Kelly, *J. Nanomater.* **2008**, *2008*, 418050.
[27] M. E. Siemens, Q. Li, R. Yang, K. A. Nelson, E. H. Anderson, M. M. Murnane, H. C. Kapteyn, *Nat. Mater.* **2010**, *9*, 26.
[28] M. V. Simkin, G. D. Mahan, *Phys. Rev. Lett.* **2000**, *84*, 927.
[29] J. Ravichandran, A. K. Yadav, R. Cheaito, P. B. Rossen, A. Soukiassian, S. J. Suresha, J. C. Duda, B. M. Foley, C.-H. Lee, Y. Zhu, A. W. Lichtenberger, J. E. Moore, D. A. Muller, D. G. Schlom, P. E. Hopkins, A. Majumdar, R. Ramesh, M. A. Zurbuchen, *Nat. Mater.* **2014**, *13*, 168.
[30] M. N. Luckyanova, J. Garg, K. Esfarjani, A. Jandl, M. T. Bulsara, A. J. Schmidt, A. J. Minnich, S. Chen, M. S. Dresselhaus, Z. Ren, E. A. Fitzgerald, G. Chen, *Science* **2012**, *338*, 936.
[31] W. S. Capinski, H. J. Maris, T. Ruf, M. Cardona, K. Ploog, D. S. Katzer, *Phys. Rev. B* **1999**, *59*, 8105.
[32] S. M. Lee, D. G. Cahill, *J. Appl. Phys.* **1997**, *81*, 2590.
[33] P. Chen, N. A. Katcho, J. P. Feser, W. Li, M. Glaser, O. G. Schmidt, D. G. Cahill, N. Mingo, A. Rastelli, *Phys. Rev. Lett.* **2013**, *111*, 115901.
[34] K. Uchinokura, T. Sekine, E. Matsuura, *J. Phys. Chem. Solids* **1974**, *35*, 171.
[35] S. V. Ovsyannikov, Y. S. Ponosov, V. V. Shchennikov, V. E. Mogilenskikh, *Phys. Status Solidi C* **2004**, *1*, 3110.

[36] N. Shulumba, O. Hellman, A. J. Minnich, *Phys. Rev. B* **2017**, *95*, 014302.
[37] B. Latour, S. Volz, Y. Chalopin, *Phys. Rev. B* **2014**, *90*, 014307.
[38] E. D. Devyatkova, I. A. Smirnov, *Sov. Phys. Solid State* **1960**, *2*, 1984.
[39] E. D. Devyatkova, I. A. Smirnov, *Sov. Phys. Solid State* **1962**, *4*, 2507.
[40] D. Gu, H. Baumgart, K. Tapily, P. Shrestha, G. Namkoong, X. Ao, F. Muller, *Nano Res.* **2011**, *4*, 164.
[41] A. J. Schmidt, *Annu. Rev. Heat Transfer* **2013**, *16*, 159.
[42] D. G. Cahill, *Rev. Sci. Instrum.* **2004**, *75*, 5119.
[43] P. E. Hopkins, J. R. Serrano, L. M. Phinney, S. P. Kearney, T. W. Grasser, C. T. Harris, *J. Heat Transfer* **2010**, *132*, 081302.
[44] A. J. Schmidt, X. Chen, G. Chen, *Rev. Sci. Instrum.* **2008**, *79*, 114902.